JACS
JOURNAL OF THE AMERICAN CHEMICAL SOCIETY
Communication
pubs.acs.org/JACS

Exploiting Copper Redox for ^{19}F Magnetic Resonance-Based Detection of Cellular Hypoxia

Da Xie, Tyler L. King, Arnab Banerjee, Vikraant Kohli, and Emily L. Que*

Department of Chemistry, The University of Texas at Austin, 105 E. 24th St Stop A5300, Austin, Texas 78712, United States

Supporting Information

ABSTRACT: We report a pair of fluorinated, redox-active copper complexes for potential use as ^{19}F MRI contrast agents for detecting cellular hypoxia. Trifluorinated Cu(II) ATSM-F_3 displays the appropriate redox potential for selective accumulation in hypoxic cells and a completely quenched ^{19}F NMR signal that is "turned on" following reduction to Cu(I). Incubation of cancer cells with CuATSM-F_3 resulted in a selective detection of ^{19}F signal in cells grown under hypoxic conditions.

Hypoxia, or biological oxygen deficiency, is a condition experienced in solid tumor cancers and other pathologies and is a result of inadequate vasculature that leads to inefficient oxygen delivery. The biochemical consequences of low oxygen levels include high expression levels of the transcription factor HIF-1 (hypoxia inducible factor 1) and increased reductive stress. Hypoxia can promote tumor proliferation, and hypoxic tissues are resistant to therapy, thus identifying these tissues is essential for planning treatment.[1,2]

To develop imaging and diagnostic agents for hypoxia detection, the increased reductive capacity of hypoxic cells has been targeted by small molecule imaging probes for a number of modalities including luminescence,[3−6] positron emission tomography (PET),[7,8] and magnetic resonance imaging (MRI).[9−15] MRI-based methods are desirable for clinical diagnostics as they can be used to image whole organisms with high anatomic detail without exposing them to ionizing radiation. A number of ^{1}H MRI-based contrast agents have been developed to detect different biological redox environments including hypoxia.[9−24] ^{19}F MRI is an emerging approach for noninvasive whole organism imaging as ^{19}F has favorable NMR properties and good biostability, and there is no detectable background ^{19}F signal in biological systems.[25−27] Organic scaffolds have shown promise for ^{19}F hypoxia imaging,[28,29] however we propose a new approach, namely to use a metal-centered redox event to modulate the ^{19}F MRI signal in response to different biological redox environments.

Our probe design is based on CuATSM, used as a radioactive $^{60/62/64}Cu^{2+}$ complex for PET imaging of hypoxia (Figure 1).[30] CuATSM is a neutral, cell permeable complex that preferentially accumulates in hypoxic cells through reduction of Cu^{2+} to Cu^{+}.[31,32] The formed Cu^{+}-ATSM species undergoes ligand dissociation, and the Cu^{+} is trapped by cellular thiols.[32] We hypothesized that by fluorinating this scaffold, we could use the conversion of paramagnetic d^9 Cu^{2+} to diamagnetic d^{10} Cu^{+} complex and ligand to create a ^{19}F MRI contrast agent that

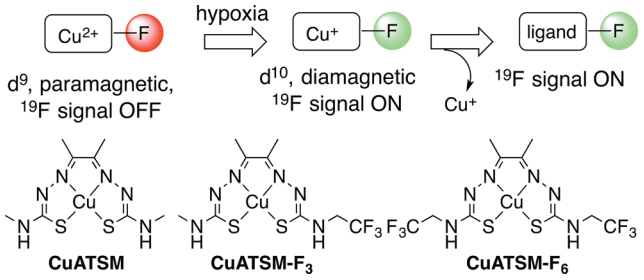

Figure 1. Design strategy for hypoxia-activated Cu^{2+}-based ^{19}F MRI sensors (top) and the chemical structures of the Cu complexes used in this study (bottom).

exhibits a "turn-on" signal in response to cellular hypoxia through a paramagnetic relaxation enhancement (PRE) mechanism.[33] The paramagnetic effect from Cu^{2+} will shorten the transverse relaxation time (T_2) of interacting ^{19}F nuclei and attenuate the intensity of their NMR/MRI signal, turning the signal "off". This is facilitated in particular by the long electronic relaxation time of Cu^{2+}.[34] Reduction of Cu^{2+} to Cu^{+} as well as further ligand dissociation will lengthen T_2, turning the signal "on". The PRE effect has been exploited in Gd^{3+}-based contrast agents,[35−38] and Ln^{3+} complexes have been explored as chemical shift MR sensors,[39] but copper-based agents are rare. These CuATSM derivatives have the additional advantage of being cell-permeable, thus enabling interrogation of the intracellular milieu.

Ligands H_2ATSM-F_3 and H_2ATSM-F_6 were readily synthesized via transamination reactions with the appropriate bis-thiosemicarbazone precursor and 2,2,2-trifluoroethanamine in 79% and 53% yields, respectively (Schemes S1 and S2). Complexation of Cu^{2+} to both ligands was achieved in good yield via reaction with $Cu(OAc)_2$ (CuATSM-F_3, 84%; CuATSM-F_6, 76%). Copper complexes were purified using C18 reverse-phase chromatography. Composition and purity were assessed using LC-MS, which confirmed the formation of 1:1 metal:ligand complexes.

Single crystals of CuATSM-F_3 and CuATSM-F_6 were grown in CH_3CN/toluene, and their X-ray structures were obtained (Figures 2, S1). Important structural parameters of the two complexes are listed in Tables S2 and S3. In both structures, the Cu^{2+} sits in a pseudosquare planar [N_2S_2] pocket. The Cu−F distances range from 5.57 to 7.23 Å, within the appropriate distance for effective PRE and fluorine signal quenching.[39]

Received: December 24, 2015
Published: February 23, 2016

DOI: 10.1021/jacs.5b13215
J. Am. Chem. Soc. 2016, 138, 2937−2940

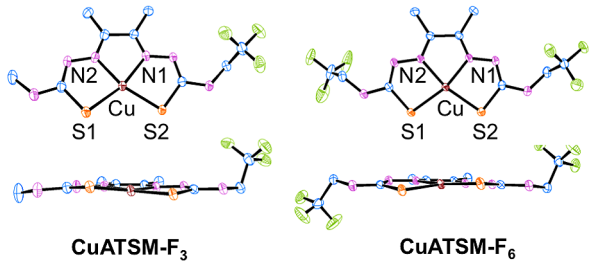

Figure 2. Molecular structures of CuATSM-F_3 and CuATSM-F_6 from single crystal X-ray diffraction. Thermal ellipsoid plots at 50% probability are shown. Solvent molecules and hydrogen atoms are omitted for clarity.

Indeed, while ligands H_2ATSM-F_3 and H_2ATSM-F_6 each displayed a prominent triplet peak in their ^{19}F NMR spectra, no observable ^{19}F NMR signal could be detected for either Cu^{2+} complex, confirming our hypothesis that Cu^{2+} could effectively quench the ^{19}F signal in these scaffolds. Prominent ^{19}F NMR signals shifted upfield relative to ligand were observed in spectra of analogous diamagnetic Ni^{2+} complexes, further supporting a role for paramagnetic Cu^{2+} in signal quenching (Figure 4A).

To study the Cu^+/Cu^{2+} redox properties of our complexes, cyclic voltammetry was performed in DMF solution for CuATSM-F_3 and CuATSM-F_6 as well as the nonfluorinated reference compound CuATSM. The results are compiled in Figure 3. The CuATSM complex showed a reversible peak for

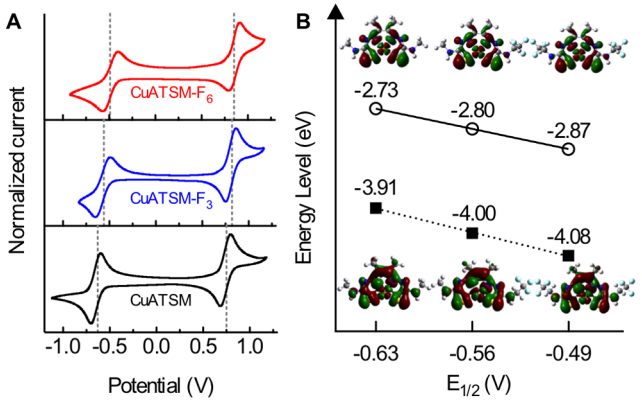

Figure 3. (A) Cyclic voltammograms of CuATSM, CuATSM-F_3, and CuATSM-F_6 (vs SCE). Half-potentials indicated by dashed gray lines. (B) Calculated unrestricted energies for the LUMO of Cu^{2+} complexes (white circles, solid line) and HOMO of the presumed anionic Cu^+ complex (dark squares, dashed line), respectively, vs the experimental half potential for Cu^+/Cu^{2+}, CuATSM on left, CuATSM-F_3 in middle and CuATSM-F_6 on right. (Inset) Calculated spatial distribution of the frontier orbitals.

the Cu^+/Cu^{2+} couple at a half-potential of −0.63 V (vs SCE), consistent with previous reports.[40] Incorporation of fluorine atoms proximal to the Cu core shifted the potential to more positive values with CuATSM-F_3 and CuATSM-F_6 displaying quasi-reversible peaks at −0.56 and −0.49 V, respectively. A Cu^+/Cu^{2+} redox potential below −0.50 V is required for effective differentiation of hypoxic and normoxic cells by ATSM type scaffolds.[40] The above values thus indicated that CuATSM-F_3 had more potential to exhibit selectivity toward hypoxic cells than CuATSM-F_6.

To better understand the redox properties of CuATSM-F_3 and CuATSM-F_6, theoretical calculations were carried out for neutral Cu^{2+} complexes and presumed anionic $[Cu^+]$ species using density functional theory (Gaussian 09), together with CuATSM as a control. The optimized structures of single Cu^{2+} complexes show good similarity, with all three complexes maintaining planar $[CuN_2S_2]$ coordination geometry (Figure S2). While slight deviation from planar Cu^{2+} coordination geometry was observed in the crystal structure, it is likely an artifact of crystal packing. The $[Cu^{2+}]$ LUMOs and $[Cu^+]$ HOMOs were further investigated since previous work demonstrated a correlation between the calculated energies of these orbitals and measured one-electron reduction potentials ($E_{1/2}$).[41] As shown in Figure 3B, for all three complexes, both orbitals exhibited partial distributions on the in-plane p orbitals of the donating ligands and d_{yz} orbital of Cu, corresponding to the metal−ligand σ^*-antibonding orbital, indicating the involvement of the metal center in the one-electron reduction of these complexes.[42,43] The energy levels of the two orbitals were plotted vs $E_{1/2}$ of Cu^+/Cu^{2+} for the three complexes, giving good linear relationships. Considering the high similarity of the coordination core of the three complexes, introducing σ-electron-withdrawing $-CF_3$ groups with a single methylene group separating them from the ATSM core lowers the energy level of both orbitals and induces the positive shift of $E_{1/2}$.[41]

Due to the promising redox properties of CuATSM-F_3 with regards to hypoxia-selectivity, we focused further studies on this compound. We monitored the reduction of this complex *in vitro* with UV−vis spectroscopy using both electrochemical reduction and chemical reduction by $Na_2S_2O_4$ (Figure S4). In both cases, the initial spectrum of CuATSM-F_3 exhibited an intense absorbance at 311 nm ($\varepsilon = 2.0 \times 10^4$ M^{-1} cm^{-1}) and a broad absorbance at 477 nm ($\varepsilon = 6.8 \times 10^3$ M^{-1} cm^{-1}), with a shoulder centered at 346 and 526 nm, respectively. This spectrum closely resembles the spectrum of CuATSM (Figure S5), suggesting a similar electronic environment.[44] Reduction by either electrochemical or chemical ($Na_2S_2O_4$) methods induced a change in color from reddish brown to yellow, together with a dramatic decrease in the absorption band at 477 nm. This band has been assigned to transitions of electronic density into the metal−ligand σ^* antibonding orbital, and this change in absorbance is consistent with a metal-centered reduction process.[44] During $Na_2S_2O_4$ reduction, absorbance increases at 310 and 400 nm were observed. These result from absorbance of $Na_2S_2O_4$ and appearance of the free ligand (Figure S6), indicating Cu^{2+} reduction is followed by ligand dissociation in aqueous solution.

To test the potential of CuATSM-F_3 to act as a ^{19}F MRI contrast agent, we monitored the reduction of this complex using ^{19}F NMR. As stated above, H_2ATSM-F_3 displayed a prominent triplet peak in its ^{19}F spectrum ($\delta = -69.96$ ppm) that was completely quenched upon complexation with Cu^{2+} and shifted upfield when complexed to diamagnetic Ni^{2+} ($\delta = -70.58$ ppm) (Figure 4A). The Cu^+ATSM-F_3 complex was generated *in situ* by combining $[Cu(CH_3CN)_4]PF_6$ and H_2ATSM-F_3 in d_6-DMSO in an inert glovebox. The ^{19}F NMR spectrum displayed two triplets at −70.18 and −70.31 ppm, consistent with formation of a dimeric $[Cu^+]$ complex as reported in similar systems (Figure S7).[45] Upon addition of one-electron reductant $CoCp_2$ to a deoxygenated anhydrous d_6-DMSO solution of CuATSM-F_3, an intense ^{19}F signal rose up from the originally silent spectrum at $\delta = -70.64$ ppm (Figure 4B). This is shifted upfield from the H_2ATSM-F_3 ligand,

DOI: 10.1021/jacs.5b13215
J. Am. Chem. Soc. 2016, 138, 2937−2940

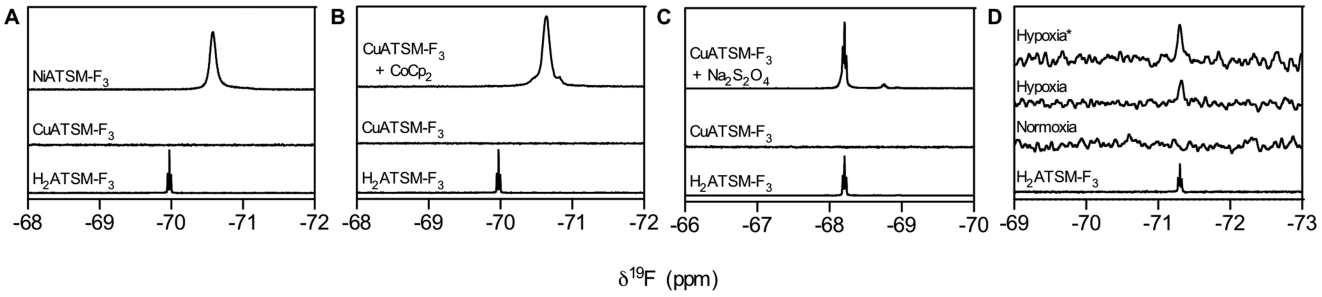

Figure 4. (A) ^{19}F NMR spectra of H_2ATSM-F_3 and its Cu^{2+} and Ni^{2+} complexes in d_6-DMSO. (B,C) One-electron reduction of CuATSM-F_3 monitored by ^{19}F NMR. CuATSM-F_3 (10 mM) was incubated at room temperature with (B) $CoCp_2$ (30 mM) in deoxygenated anhydrous d_6-DMSO for 1 h or (C) $Na_2S_2O_4$ (excess) in 60% DMSO/30% HEPES (pH 7, 20 mM)/10% D_2O mixture for 5 min. (D) Selective detection of hypoxia in MCF-7 cells through ^{19}F NMR using CuATSM-F_3. MCF-7 cells were incubated with CuATSM-F_3 (100 μM) for 2 h under aerobic and hypoxic environment, respectively, and cell lysate was diluted by half with DMSO and subjected to ^{19}F NMR scans for 1600 or 2048 times (marked with *).

suggesting a transition from a paramagnetic Cu^{2+} state to a diamagnetic Cu^{+} state of the complex. To better mimic a biological environment, the reduction was further performed in a mixture of DMSO and HEPES buffer, with $Na_2S_2O_4$ as reductant. Post-reduction, the system displayed a weak triplet at $\delta = -68.80$ ppm and a sharp triplet at $\delta = -68.21$ ppm, which matched up well with the ATSM-F_3 ligand (Figure 4C). The downfield peak is consistent with a reduction followed by ligand dissociation, while the upfield peak we ascribed to formation of a [Cu^{+}] species. This observation is similar to what occurred when water was added to the *in situ* generated Cu^{+}ATSM-F_3 complex (Figure S8).

We further tested the potential for CuATSM-F_3 to differentiate normoxic (20% O_2) and hypoxic (1% O_2) conditions in cell culture using MCF-7 human breast cancer cells. Total cellular uptake was assessed using ICP-OES (Figure S9). After a 2 h incubation of the complex at 100 μM concentration, MCF-7 cells showed sufficient uptake of the neutral Cu^{2+} complex (10^{-15} mol/cell), with a 73% enhancement in complex accumulation in cells grown under hypoxic conditions vs those grown under normoxic conditions. Finally, we employed ^{19}F NMR to confirm hypoxia-selective reduction of CuATSM-F_3 within cells for an exclusive "switch on" in the context of ^{19}F NMR/MRI. Cells were cultured with 100 μM CuATSM-F_3 for 2 h under hypoxic and normoxic conditions and lysed under the same oxygen levels. Indeed, a ^{19}F NMR signal was observed at −71.3 ppm in lysate from cells grown under hypoxic conditions (S/N ∼ 6:1 compared to the calculated spectral noise level). In the absence of cells, no signal was observed when CuATSM-F_3 was incubated in hypoxic culture medium, suggesting a requirement for cellular machinery to reduce the complex (Figure S10). Importantly, in cells grown under normoxic conditions, the spectrum of the cell lysate remained silent (Figure 4D). Incubation of cells with H_2ATSM-F_3 returned a triplet that overlapped with the peak observed in hypoxic cells, suggesting ligand dissociation as the prevailing mechanism for trapping this complex. These results suggest a potential for this class of compounds to act as reporters to track hypoxic cells using ^{19}F MRI.

This proof-of-concept study demonstrates the potential for cell-permeable fluorinated CuATSM scaffolds as redox-active platforms for detecting cellular hypoxia using ^{19}F MRI. Incorporation of fluorine atoms proximal to the Cu^{2+} allowed efficient quenching of the ^{19}F NMR signal via the PRE effect, suggesting that ^{19}F signal should be completely off until d^9 Cu^{2+} is reduced to d^{10} Cu^{+} in hypoxic cells and the signal is turned on. The measured Cu^{+}/Cu^{2+} redox potential of CuATSM-F_3 is well within the regime for hypoxia selectivity, and we were able to monitor "turn-on" of the ^{19}F signal in the presence of chemical reductants and, importantly, in cells grown under hypoxic conditions. Ongoing and future studies include further improving the fluorine density, redox properties, water solubility, and hypoxia targeting of these scaffolds with the aim of developing probes that can be used for *in vivo* imaging of hypoxia.

■ ASSOCIATED CONTENT

Ⓢ Supporting Information

The Supporting Information is available free of charge on the ACS Publications website at DOI: 10.1021/jacs.5b13215.

(CIF)

(CIF)

Experimental details and data (PDF)

■ AUTHOR INFORMATION

Corresponding Author

*emilyque@cm.utexas.edu

Notes

The authors declare no competing financial interest.

■ ACKNOWLEDGMENTS

This work was funded by start-up funds from the University of Texas at Austin (E.Q.), a grant from the Welch Foundation (F-1883) (E.Q.), and a Banks Summer Fellowship from the UT Department of Chemistry (D.X.). We gratefully acknowledge Prof. Bradley Holliday for helpful discussions and providing access to Gaussian, Dr. Vincent Lynch for X-ray crystallography support, Prof. Michael Rose for glovebox use, and Prof. Blerta Xhemalce for providing MCF-7 cells. We thank Dr. Omar Qazi for cell culture guidance and Que group members for discussions.

■ REFERENCES

(1) Wilson, W. R.; Hay, M. P. *Nat. Rev. Cancer* **2011**, *11*, 393.
(2) Vaupel, P.; Mayer, A.; Hockel, M. *Methods Enzymol.* **2004**, *381*, 335.
(3) Takahashi, S.; Piao, W.; Matsumura, Y.; Komatsu, T.; Ueno, T.; Terai, T.; Kamachi, T.; Kohno, M.; Nagano, T.; Hanaoka, K. *J. Am. Chem. Soc.* **2012**, *134*, 19588.

DOI: 10.1021/jacs.5b13215
J. Am. Chem. Soc. 2016, 138, 2937−2940

(4) Kiyose, K.; Hanaoka, K.; Oushiki, D.; Nakamura, T.; Kajimura, M.; Suematsu, M.; Nishimatsu, H.; Yamane, T.; Terai, T.; Hirata, Y.; Nagano, T. *J. Am. Chem. Soc.* **2010**, *132*, 15846.
(5) Li, Y.; Sun, Y.; Li, J.; Su, Q.; Yuan, W.; Dai, Y.; Han, C.; Wang, Q.; Feng, W.; Li, F. *J. Am. Chem. Soc.* **2015**, *137*, 6407.
(6) Zhao, Q.; Zhou, X.; Cao, T.; Zhang, K. Y.; Yang, L.; Liu, S.; Liang, H.; Yang, H.; Li, F.; Huang, W. *Chem. Sci.* **2015**, *6*, 1825.
(7) Lopci, E.; Grassi, I.; Chiti, A.; Nanni, C.; Cicoria, G.; Toschi, L.; Fonti, C.; Lodi, F.; Mattioli, S.; Fanti, S. *Am. J. Nucl. Med. Mol. Imaging* **2014**, *4*, 365.
(8) Yang, D. J.; Wallace, S.; Cherif, A.; Li, C.; Gretzer, M. B.; Kim, E. E.; Podoloff, D. A. *Radiology* **1995**, *194*, 795.
(9) Di Gregorio, E.; Ferrauto, G.; Gianolio, E.; Lanzardo, S.; Carrera, C.; Fedeli, F.; Aime, S. *ACS Nano* **2015**, *9*, 8239.
(10) Iwaki, S.; Hanaoka, K.; Piao, W.; Komatsu, T.; Ueno, T.; Terai, T.; Nagano, T. *Bioorg. Med. Chem. Lett.* **2012**, *22*, 2798.
(11) Pacheco-Torres, J.; López-Larrubia, P.; Ballesteros, P.; Cerdán, S. *NMR Biomed.* **2011**, *24*, 1.
(12) Tanabe, K.; Harada, H.; Narazaki, M.; Tanaka, K.; Inafuku, K.; Komatsu, H.; Ito, T.; Yamada, H.; Chujo, Y.; Matsuda, T.; Hiraoka, M.; Nishimoto, S.-i. *J. Am. Chem. Soc.* **2009**, *131*, 15982.
(13) Rojas-Quijano, F. A.; Tircso, G.; Tircsone Benyo, E.; Baranyai, Z.; Tran Hoang, H.; Kalman, F. K.; Gulaka, P. K.; Kodibagkar, V. D.; Aime, S.; Kovacs, Z.; Sherry, A. D. *Chem. - Eur. J.* **2012**, *18*, 9669.
(14) Do, Q. N.; Ratnakar, J. S.; Kovacs, Z.; Sherry, A. D. *ChemMedChem* **2014**, *9*, 1116.
(15) Gulaka, P. K.; Rojas-Quijano, F.; Kovacs, Z.; Mason, R. P.; Sherry, A. D.; Kodibagkar, V. D. *JBIC, J. Biol. Inorg. Chem.* **2014**, *19*, 271.
(16) Yu, M.; Ambrose, S. L.; Whaley, Z. L.; Fan, S.; Gorden, J. D.; Beyers, R. J.; Schwartz, D. D.; Goldsmith, C. R. *J. Am. Chem. Soc.* **2014**, *136*, 12836.
(17) Loving, G. S.; Mukherjee, S.; Caravan, P. *J. Am. Chem. Soc.* **2013**, *135*, 4620.
(18) Ratnakar, S. J.; Viswanathan, S.; Kovacs, Z.; Jindal, A. K.; Green, K. N.; Sherry, A. D. *J. Am. Chem. Soc.* **2012**, *134*, 5798.
(19) Tsitovich, P. B.; Spernyak, J. A.; Morrow, J. R. *Angew. Chem., Int. Ed.* **2013**, *52*, 13997.
(20) Aime, S.; Botta, M.; Gianolio, E.; Terreno, E. *Angew. Chem., Int. Ed.* **2000**, *39*, 747.
(21) Raghunand, N.; Jagadish, B.; Trouard, T. P.; Galons, J.-P.; Gillies, R. J.; Mash, E. A. *Magn. Reson. Med.* **2006**, *55*, 1272.
(22) Ekanger, L. A.; Polin, L. A.; Shen, Y.; Haacke, E. M.; Martin, P. D.; Allen, M. J. *Angew. Chem., Int. Ed.* **2015**, *54*, 14398.
(23) Szabo, I.; Crich, S. G.; Alberti, D.; Kalman, F. K.; Aime, S. *Chem. Commun.* **2012**, *48*, 2436.
(24) Liu, G.; Li, Y.; Pagel, M. D. *Magn. Reson. Med.* **2007**, *58*, 1249.
(25) Ruiz-Cabello, J.; Barnett, B. P.; Bottomley, P. A.; Bulte, J. W. M. *NMR Biomed.* **2011**, *24*, 114.
(26) Tirotta, I.; Dichiarante, V.; Pigliacelli, C.; Cavallo, G.; Terraneo, G.; Bombelli, F. B.; Metrangolo, P.; Resnati, G. *Chem. Rev.* **2015**, *115*, 1106.
(27) Terreno, E.; Castelli, D. D.; Viale, A.; Aime, S. *Chem. Rev.* **2010**, *110*, 3019.
(28) Liu, S.; Shah, S. J.; Wilmes, L. J.; Feiner, J.; Kodibagkar, V. D.; Wendland, M. F.; Mason, R. P.; Hylton, N.; Hopf, H. W.; Rollins, M. D. *Magn. Reson. Med.* **2011**, *66*, 1722.
(29) Yu, J. X.; Kodibagkar, V. D.; Cui, W.; Mason, R. P. *Curr. Med. Chem.* **2005**, *12*, 819.
(30) Fujibayashi, Y.; Taniuchi, H.; Yonekura, Y.; Ohtani, H.; Konishi, J.; Yokoyama, A. *J. Nucl. Med.* **1997**, *38*, 1155.
(31) Vavere, A. L.; Lewis, J. S. *Dalton Trans.* **2007**, 4893.
(32) Zeglis, B. M.; Houghton, J. L.; Evans, M. J.; Viola-Villegas, N.; Lewis, J. S. *Inorg. Chem.* **2014**, *53*, 1880.
(33) Clore, G. M.; Iwahara, J. *Chem. Rev.* **2009**, *109*, 4108.
(34) Jahnke, W., The Use of Spin Labels in NMR-Supported Lead Finding and Optimization. In *BioNMR in Drug Research*; Wiley-VCH Verlag GmbH & Co. KGaA: Weinheim, 2003; p 341.
(35) Mizukami, S.; Takikawa, R.; Sugihara, F.; Hori, Y.; Tochio, H.; Wälchli, M.; Shirakawa, M.; Kikuchi, K. *J. Am. Chem. Soc.* **2008**, *130*, 794.
(36) Mizukami, S.; Takikawa, R.; Sugihara, F.; Shirakawa, M.; Kikuchi, K. *Angew. Chem., Int. Ed.* **2009**, *48*, 3641.
(37) Mizukami, S.; Matsushita, H.; Takikawa, R.; Sugihara, F.; Shirakawa, M.; Kikuchi, K. *Chem. Sci.* **2011**, *2*, 1151.
(38) Kitamura, N.; Hiraoka, T.; Tanaka, K.; Chujo, Y. *Bioorg. Med. Chem.* **2012**, *20*, 4668.
(39) Harvey, P.; Kuprov, I.; Parker, D. *Eur. J. Inorg. Chem.* **2012**, *2012*, 2015.
(40) Dearling, J. L.; Lewis, J. S.; Mullen, G. E.; Welch, M. J.; Blower, P. J. *JBIC, J. Biol. Inorg. Chem.* **2002**, *7*, 249.
(41) Holland, J. P.; Green, J. C.; Dilworth, J. R. *Dalton Trans.* **2006**, 783.
(42) Holland, J. P.; Barnard, P. J.; Collison, D.; Dilworth, J. R.; Edge, R.; Green, J. C.; McInnes, E. J. L. *Chem. - Eur. J.* **2008**, *14*, 5890.
(43) Castle, T. C.; Maurer, R. I.; Sowrey, F. E.; Went, M. J.; Reynolds, C. A.; McInnes, E. J. L.; Blower, P. J. *J. Am. Chem. Soc.* **2003**, *125*, 10040.
(44) Holland, J. P.; Aigbirhio, F. I.; Betts, H. M.; Bonnitcha, P. D.; Burke, P.; Christlieb, M.; Churchill, G. C.; Cowley, A. R.; Dilworth, J. R.; Donnelly, P. S.; Green, J. C.; Peach, J. M.; Vasudevan, S. R.; Warren, J. E. *Inorg. Chem.* **2007**, *46*, 465.
(45) Cowley, A. R.; Dilworth, J. R.; Donnelly, P. S.; Labisbal, E.; Sousa, A. *J. Am. Chem. Soc.* **2002**, *124*, 5270.

DOI: 10.1021/jacs.5b13215
J. Am. Chem. Soc. 2016, 138, 2937−2940